[Electronic Supplementary Information to accompany:]

Cyclic metalloporphyrin dimers and tetramers: tunable shape-selective hosts for fullerenes

Byungman Kang,[a,b] Ryan K. Totten,[a,b] Mitchell H. Weston,[a] Joseph T. Hupp[a] and SonBinh T. Nguyen*[,a]

[a]*Department of Chemistry and International Institute for Nanotechnology, Northwestern University, 2145 Sheridan Road, Evanston, Illinois 60208-3113, USA.* [b]*Authors contributed equally*

Table of Contents *Page number*

I. General Information. ^{1}H and ^{13}C NMR spectra were recorded on either a Varian INOVA 500 FT-NMR (499.6 MHz for ^{1}H, 125.6 MHz for ^{13}C) or a Varian Mercury 400 FT-NMR spectrometer (400.6 MHz for ^{1}H, 100.7 MHz for ^{13}C). ^{1}H NMR data are reported as follows: chemical shift (multiplicity (br s = broad singlet, s = singlet, d = doublet, t = triplet, q = quartet, and m = multiplet), coupling constant and integration). ^{1}H and ^{13}C chemical shifts are reported in ppm downfield from tetramethylsilane (TMS, δ scale) using residual solvent resonances as internal standards.

Matrix-assisted laser desorption ionization time-of-flight (MALDI-ToF) mass spectra were recorded on a Bruker Autoflex III MALDI spectrometer using either reflective positive or linear negative ionization method with dithranol matrix. Electrospray-ionization mass spectrometric (ESIMS) data were obtained by staff members in the Integrated Molecular Structure Education and Research Center (IMSERC) at Northwestern University (Evanston, IL, USA).

UV-vis spectra were obtained in toluene on a Varian Cary 500 spectrophotometer, unless otherwise noted. Fluorescence emission spectra were obtained in toluene on a Jobin Yvon FluoroLog fluorometer (λ_{ex} = 419 nm, λ_{em} = 500 – 800 nm, slit width = 3 nm) (HORIBA Jobin Yvon Inc., Edison, NJ, USA).

II. General procedures and materials. All air- or water-sensitive reactions were carried out under nitrogen using oven-dried glassware. All synthetic experiments concerning porphyrin and porphyrin derivatives were carried out under light-deficient conditions: the hood lights were turned off and the reaction flasks are covered with aluminum foil to further minimize light exposure. Isolated porphyrin products were stored at low temperatures (-10 °C) in foil-covered vials. All flash-column chromatography was carried out using silica gel (MP Silitech 60-200 mesh) under a positive pressure of nitrogen, unless otherwise noted. Analytical thin layer chromatography (TLC) was

performed using glass-backed silica gel 60 F_{254} plates (Merck EMD-571507). Visualization of the TLC results was achieved either by observation under UV light (254 nm), or via treatment with 10 wt% phosphomolybdic acid in ethanol followed by heating.

Cyclic cofacial porphyrin dimers **A1-A6**,[S1] unsaturated Zn(porphyrin) tetramer (**Zn-PP**)$_4$,[S2] [5,10,15,20-tetrakis(4-(4′-pyridyl)-3,5-(dimethyl)phenyl)]porphine (**Py-MesP**),[S2] [5,15-bis(4-pyridyl)-10,20-diphenyl]porphine (**H$_2$-DPyDPP**),[S3] [[5,15-bis(4-pyridyl)-10,20-diphenyl]porphinato]zinc(II) (**Zn^{II}-DPyDPP**),[S4] and [[5,15-bis(4-pyridyl)-10,20-diphenyl]porphinato]cobalt(II) (**Co^{II}-DPyDPP**)[S5] were synthesized according to published procedures. Tetrahydrofuran and dichloromethane (Fisher Scientific) were dried over neutral alumina in a Dow-Grubbs solvent system[S6] installed by Glass Contours (now SG Water, Nashua, NH, USA). All other reagents and solvents were purchased from the Aldrich Chemical Company (Milwaukee, WI, USA) and used without further purification. Deuterated solvents were purchased from Cambridge Isotope Laboratories (Andover, MA, USA) and used without further purification.

III. Preparation of metalloporphyrin "dividers".

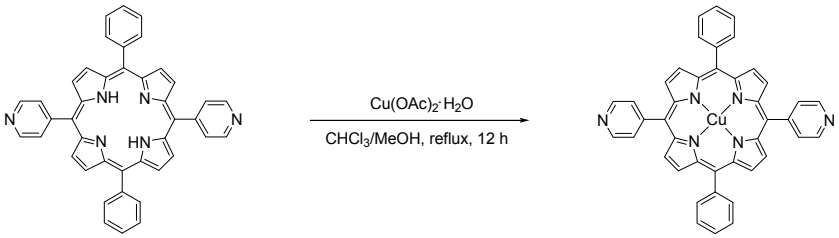

[[5,15-bis(4-pyridyl)-10,20-diphenyl]porphinato]copper(II) (Cu^{II}-DPyDPP). In a 100-mL round-bottom flask equipped with a reflux condenser, a saturated solution of $Cu(OAc)_2 \cdot H_2O$ (65 mg, 326 μmol) in MeOH (10 mL) was added to a solution of **H$_2$-DPyDPP** (50 mg, 81 μmol) in $CHCl_3$ (30 mL). The reaction mixture was refluxed for 12 h, cooled down to room temperature, and evaporated to dryness under reduced pressure. The solid was washed with MeOH (3 × 20 mL) and dried in vacuo to yield **Cu^{II}-DPyDPP** as a pink powder (53 mg, 78 μmol, 96% yield). ^{1}H NMR (499.6 MHz, $CDCl_3$): δ 7.53 (br, 10H, α-pyridyl-*H* and Ar-*H*), 7.69 (br, 8H, β-pyridyl-*H* and Ar-*H*), 8.98 (br, 8H, β-*H*). MALDI-ToF (reflective positive mode): Calcd for $C_{42}H_{26}N_6Cu$: 678.24, found: *m/z* 678.02 $[M]^+$. UV-vis (nm, ($\varepsilon \times 10^4$ /M^{-1}cm^{-1})): 416 (27.2), 537 (1.3).

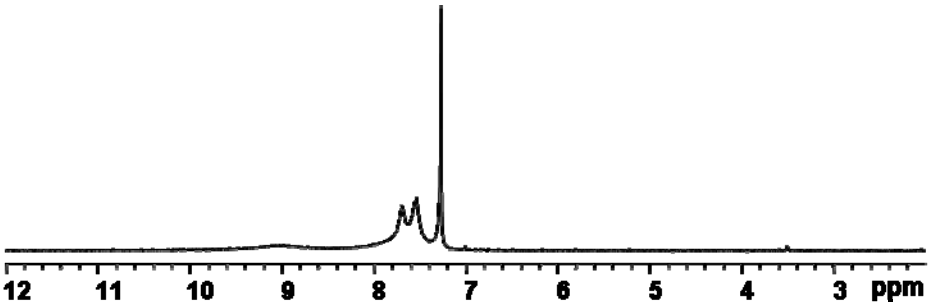

Fig. S1 The ^{1}H NMR spectrum of **Cu^{II}-DPyDPP**. This spectrum is similar to that observed for [*meso*-tetrakisphenylporphinato]copper(II) (**Cu^{II}-TPP**).[S7]

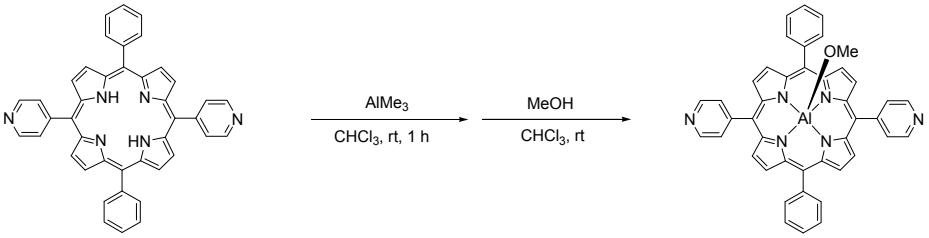

H_2-DPyDPP **MeO-Al^{III}-DPyDPP**

[[5,15-bis(4-pyridyl)-10,20-diphenyl]porphinato]aluminum(III) methoxide (MeO-Al^{III}-DPyDPP). Under a N_2 atmosphere, a 50-mL Schlenk flask equipped with a magnetic stir bar was loaded with a solution of **H_2-DPyDPP** (40 mg, 65 μmol) in anhydrous $CHCl_3$ (20 mL). A solution of $AlMe_3$ (97 μL, 195 μmol, 2.0 M in heptane) was then added to the reaction mixture using a gas-tight syringe under N_2. After stirring for 1 h under N_2, MeOH (10 mL) was added to quench the reaction and the mixture was evaporated to dryness under reduced pressure. The residue was subject to size-exclusion chromatography (column dimensions = 30 mm × 250 mm, Bio-Rad Bio-Beads S-X1, eluent = $CHCl_3$/MeOH 20:1 v/v) to afford **MeO-Al^{III}-DPyDPP** as a purple solid (40 mg, 59 μmol, 91% yield). ^{1}H NMR (499.6 MHz, $CDCl_3/CD_3OD$): δ 3.33 (s, 3H, OC*H*$_3$), 7.75 (m, 6H, Ar-*H*), 8.15 (m, 8H, α-pyridyl-*H* and Ar-*H*), 8.83 (d, J = 6.0 Hz, 4H, β-pyridyl-*H*), 8.89 (d, J = 4.4 Hz, 4H, β-*H*), 9.03 (d, J = 4.8 Hz, 4H, β-*H*). ESIMS (positive mode): Calcd for $C_{43}H_{29}N_6OAl$: 672.22, found: *m/z* 672.89 $[M]^+$. UV-vis (nm, ($\varepsilon \times 10^4$ /$M^{-1}cm^{-1}$)): 417 (11.0), 549 (0.5).

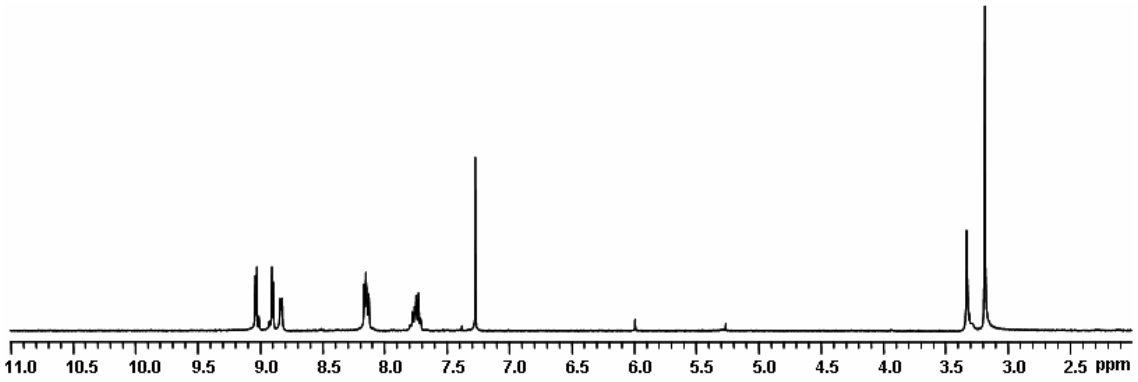

Fig. S2 The ^{1}H NMR spectrum of **MeO-Al^{III}-DPyDPP**.

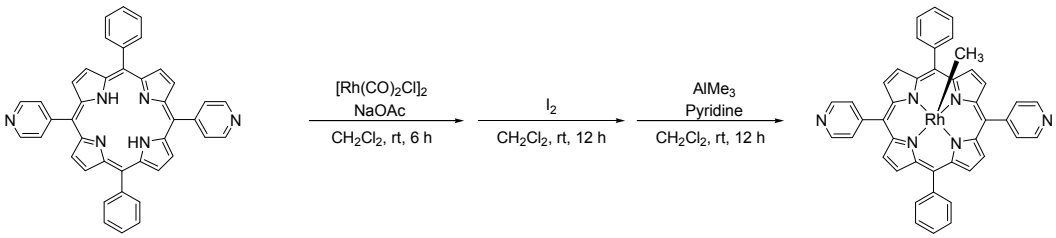

H_2-DPyDPP **Rh^{III}-CH_3-DPyDPP**

Methyl[[5,15-bis(4-pyridyl)-10,20-diphenyl]porphinato]rhodium(III) (Me-Rh^{III}-DPyDPP). This compound was synthesized following a modified literature procedure.[S8] In a 100-mL round-bottom flask equipped with a magnetic stir bar, NaOAc (359 mg, 4.38 mmol) was added to a mixture of **H_2-DPyDPP** (90 mg, 146 μmol) and $[Rh(CO)_2Cl]_2$ (227 mg, 584 μmol) in anhydrous CH_2Cl_2 (50 mL). After stirring for 6 h under N_2 atmosphere at room temperature, I_2 (222 mg, 875 μmol) was added as a solid and the reaction was stirred for an additional 12 h at room temperature. The reaction mixture was filtered through a pad of silica gel, which was then washed with a

mixture of CH_2Cl_2/MeOH/pyridine (2 × 30 mL, 40:1:1 v/v/v). To a mixture of the residue and pyridine (7.5 mg, 95 μmol) in anhydrous CH_2Cl_2 (50 mL), $AlMe_3$ (379 μL of a 2.0 M solution in heptane, 758 μmol,) was immediately added under N_2 atmosphere, and the reaction mixture was stirred for 12 h at room temperature. MeOH (20 mL) was added to quench the reaction and the mixture was evaporated to dryness under reduced pressure. The resulting residue was subjected to silica gel column chromatography (column dimensions = 20 mm × 200 mm, eluent = $CHCl_3$/MeOH/pyridine = 30:1:1 v/v/v) to yield **Me-Rh^{III}-DPyDPP** as a red solid (54 mg, 74 μmol, 51% yield). ^{1}H NMR (499.6 MHz, $CDCl_3$/pyridine-d_5): δ -6.71 (s, 3H, Rh-CH_3), 6.75 (d, J = 7.6 Hz, 4H, α-pyridyl-*H*), 7.06 (d, J = 7.6 Hz, 4H, β-pyridyl-*H*), 7.67 (m, 6H, Ar-*H*), 8.05 (m, 4H, Ar-*H*), 8.61 (m, 8H, β-*H*). ESIMS (positive mode): Calcd for $C_{43}H_{29}N_6Rh$: 732.15, found: *m/z* 733.47 $[M + H]^+$. UV-vis (nm, (ε × 10^4 /$M^{-1}cm^{-1}$)): 414 (1.7), 523 (0.2).

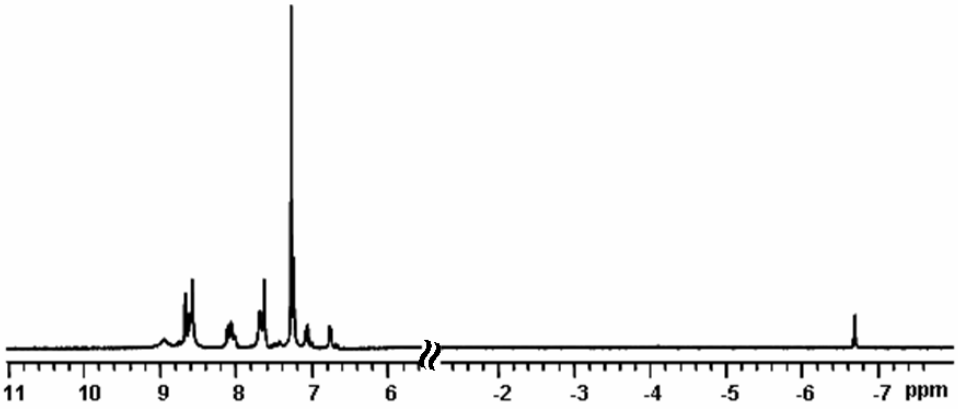

Fig. S3 The ^{1}H NMR spectrum of **Me-Rh^{III}-DPyDPP**.

IV. Preparation of the saturated (Zn-PP)$_4$ tetramer.

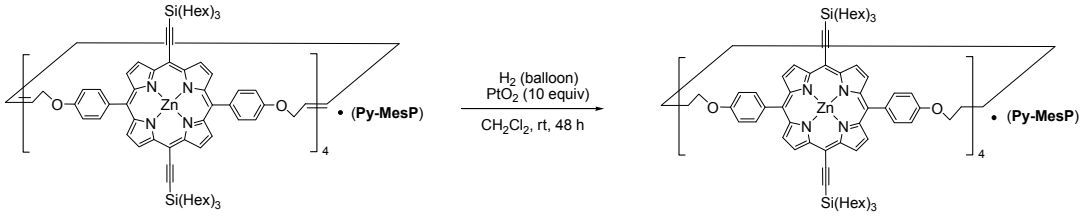

Unsaturated (Zn-PP)$_4$·(Py-MesP) **Saturated (Zn-PP)$_4$·(Py-MesP)**

Saturated (Zn-PP)$_4$·(Py-MesP). In a 25-mL two-neck, round-bottom flask equipped with a magnetic stir bar, PtO_2 (9.3 mg, 40.9 μmol) was added to a solution of unsaturated (**Zn-PP**)$_4$·(**Py-MesP**) (25 mg, 4.1 μmol) in anhydrous CH_2Cl_2 (10 mL). After stirring for 48 h under H_2 (balloon) at room temperature, the reaction mixture was filtered through a pad of Celite and evaporated to dryness by rotary evaporation. The resulting residue was subjected to silica gel column chromatography (column dimensions = 20 mm × 200 mm, eluent = CH_2Cl_2/hexanes 1:1.5 v/v) to yield the saturated (**Zn-PP**)$_4$·(**Py-MesP**) as a purple solid (22 mg, 3.6 μmol, 88% yield). ^{1}H NMR (499.6 MHz, $CDCl_3$): δ -3.40 (s, 2H, N*H*), 0.88 (m, 72H, ^{n}Hex CH_3), 0.99 (m, 48H, ^{n}Hex CH_2), 1.27-1.37 (m, 96H, ^{n}Hex CH_2), 1.52 (m, 48H, ^{n}Hex CH_2), 1.75 (m, 48H, ^{n}Hex CH_2), 1.83 (m, 16H, CH_2), 2.15 (m, 16H, CH_2CH$_2$O), 2.75 (d, J = 4.0 Hz, 8H, α-pyridyl-*H*), 4.38 (m, 16H, CH$_2$CH_2O), 5.59 (d, J = 4.0 Hz, 8H, β-pyridyl-*H*), 7.28 (s, 16H, Ar-*H*), 7.38 (br s, 8H, Py-MesP Ar-*H*), 8.15 (br s, 8H, Py-MesP β-*H*), 8.29 (s, 16H, Ar-*H*), 8.97 (d, J = 3.2 Hz, 16H, β-*H*), 9.68 (d, J = 4.0 Hz, 16H, β-*H*). MALDI-ToF (linear negative mode): Calcd for $C_{320}H_{440}N_{16}O_8Si_8Zn_4$ [M -

(Py-MesP)]$^-$: 5125.26, found: *m/z* 5125.16 [M - (Py-MesP)]$^-$. UV-vis (nm, (ε × 10^5 /$M^{-1}cm^{-1}$)): 420 (3.1), 440 (5.6), 454 (3.6), 597 (0.2), 645 (0.7).

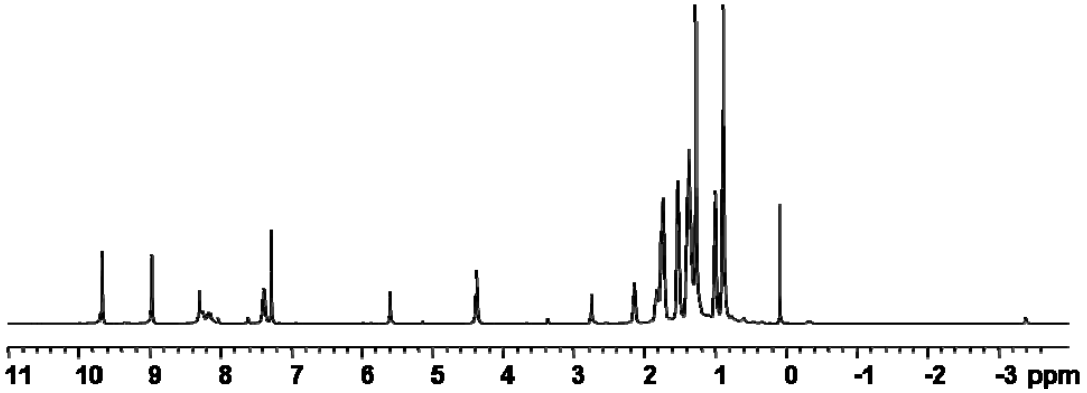

Fig. S4 The ^{1}H NMR spectrum of saturated (**Zn-PP**)$_4$·(**Py-MesP**).

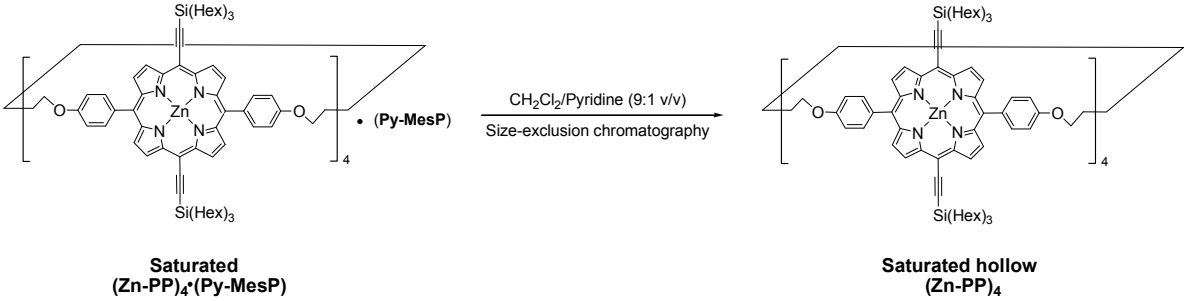

Saturated hollow (**Zn-PP**)$_4$. Saturated (**Zn-PP**)$_4$·(**Py-MesP**) (20 mg, 3.2 μmol) was dissolved in a mixture of CH_2Cl_2/pyridine (9:1 v/v) and then subjected to size-exclusion chromatography (column dimensions = 20 mm × 200 mm, Bio-Rad Bio-Beads S-X1, eluent = CH_2Cl_2/pyridine 9:1 v/v). Template-free saturated hollow (**Zn-PP**)$_4$ was collected from a dark purple band and the volatiles were removed under reduced pressure. To remove excess pyridine completely, the isolated purple solid was evacuated for 4 h at 60 ºC. Yield = 16 mg (3.1 μmol, 97%). ^{1}H NMR (499.6 MHz, CDCl3): δ 0.89 (m, 48H, ^{n}Hex CH_3), 0.98 (m, 24H, ^{n}Hex CH_3), 1.27-1.43 (m, 160H, ^{n}Hex CH_2), 1.52 (m, 40H, ^{n}Hex CH_2), 1.71 (m, 40H, ^{n}Hex CH_2), 1.81 (m, 16H, CH_2), 2.13 (m, 16H, CH_2CH$_2$O), 4.37 (m, 16H, CH$_2$CH_2O), 7.34 (d, *J* = 7.6 Hz, 16H, Ar-*H*), 8.07 (d, *J* = 7.6 Hz , 16H, Ar-*H*), 8.85 (d, *J* = 4.0 Hz, 16H, β-*H*), 9.45 (d, *J* = 3.2 Hz, 16H, β-*H*). MALDI-ToF (linear negative mode): Calcd for $C_{320}H_{440}N_{16}O_8Si_8Zn_4$: 5125.26, found: *m/z* 5125.75 [M]$^-$. UV-vis (nm, (ε × 10^5 /$M^{-1}cm^{-1}$)): 440 (23.2), 537 (0.3), 580 (0.9), 628 (2.4).

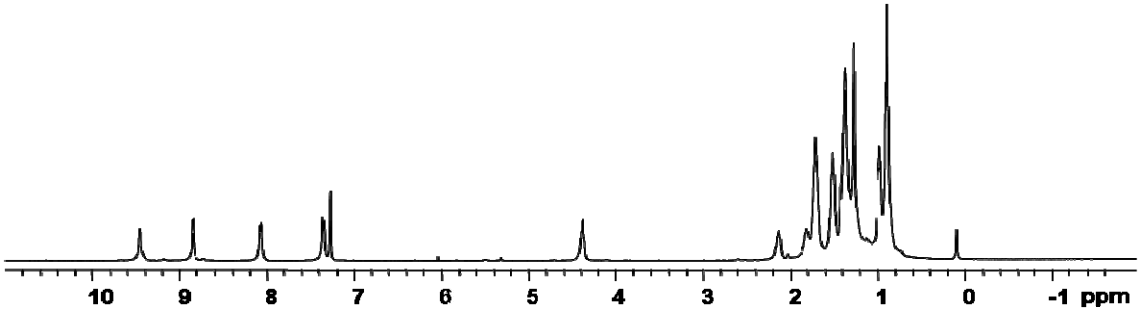

Fig. S5 The ^{1}H NMR spectrum of saturated hollow (**Zn-PP**)$_4$.

V. Evaluation of association constants by UV-vis and fluorescence titrations. The UV-vis spectrophotometric titrations of cofacial porphyrin dimers were conducted by progressively adding small aliquots (10 μL) of fullerene solution ([C_{60}] = 0.5, 0.9, 3, and 6 × 10^{-4} M or [C_{70}] = 2 and 4 × 10^{-5} M) in toluene, using a 25-μL microliter syringe, to a cuvette containing the dimer solution (2.3 mL of a 0.5 × 10^{-6} M solution) in toluene. To minimize the change of the solution volume, the maximum total added volume for all aliquots of the fullerene was less than 250 μL.

In the case of the bisected Zn(porphyrin) tetramer, prior incorporation of the divider into the hollow (**Zn-PP**)$_4$ is required before carrying out the UV-vis titration experiments. To this end, an aliquot (10 μL) of the **M-DPyDPP** divider in toluene (0.12 × 10^{-3} M; note: a mixture of toluene/MeOH (45:1 v/v) is required for the **MeO-Al^{III}-DPyDPP** and **Me-Rh^{III}-DPyDPP** dividers) was added to a cuvette containing either unsaturated or saturated (**Zn-PP**)$_4$ solution (2.3 mL of a 0.5 × 10^{-6} M solution) in toluene. The mixture was then stirred at room temperature for 5 min, resulting in the appearance of a new peak in the Q band (644 nm) indicative of the encapsulation of the divider. Titration of the resulting bisected Zn(porphyrin) tetramer with fullerenes was carried out under the same conditions as described above for the dimer. As an example for the analysis of UV-vis titration data, the absorbances (A) of a cofacial porphyrin dimer **A1** in the presence and absence of the fullerene was plotted against [C_{60}] or [C_{70}] (Fig. S6). The association constants (K_a) for C_{60} and C_{70} were derived using the Marquardt least-squares minimization based on the 1:1 complexation model.[S9]

Similarly, the fluorescence titrations were carried out by progressively adding small aliquots (10 μL) of fullerene solution to a quartz fluorescence cuvette containing the dimer solution (1 mL of a 0.5 × 10^{-6} M solution) in toluene. The solution was excited at 419 nm and the fluorescent emission intensity was recorded from 500 to 800 nm after each addition of the fullerene. A plot of intensity versus [C_{60}] or [C_{70}] was carried out to determine the K_a value by the nonlinear fitting method described above (Figs. S11 and S13).

Interestingly, in the UV-vis titration experiments, addition of incremental amounts of C_{60} and C_{70} to a solution of **A6** caused a bathochromic shift along with an increase in absorption of the Soret band (Fig. S12). This spectral feature is inconsistent with the behaviors observed for the interactions of fullerenes with **A1**-**A5** and other porphyrin hosts reported thus far.[S10,11] While we are unable to explain this result, fluorescence titrations clearly demonstrate the existence of strong π-π interactions between the fullerene and **A6**: the fluorescence emission of **A6** is efficiently quenched upon addition of C_{60} and C_{70} (Fig. S13).[S12-15] The nonlinear fit of the fluorescence titration data to the 1:1 binding model also gave K_a values that are comparable to those of the absorption titrations (~2.0 × 10^6 M^{-1} for C_{60} and ~8.5 × 10^6 M^{-1} for C_{70}, see Figs. S12 and S13). Analysis of the variable-temperature ^{13}C NMR spectra of a mixture of **A6** and C_{60} (3 equiv) in toluene-d_8 provided additional evidence supporting the association of **A6** with fullerene (Fig. S22). The coalescence temperature arising from the fast exchange of bound and unbound C_{60} was observed to be ~296 K, which is much higher than that for **A1** (253 K, Fig. S21).

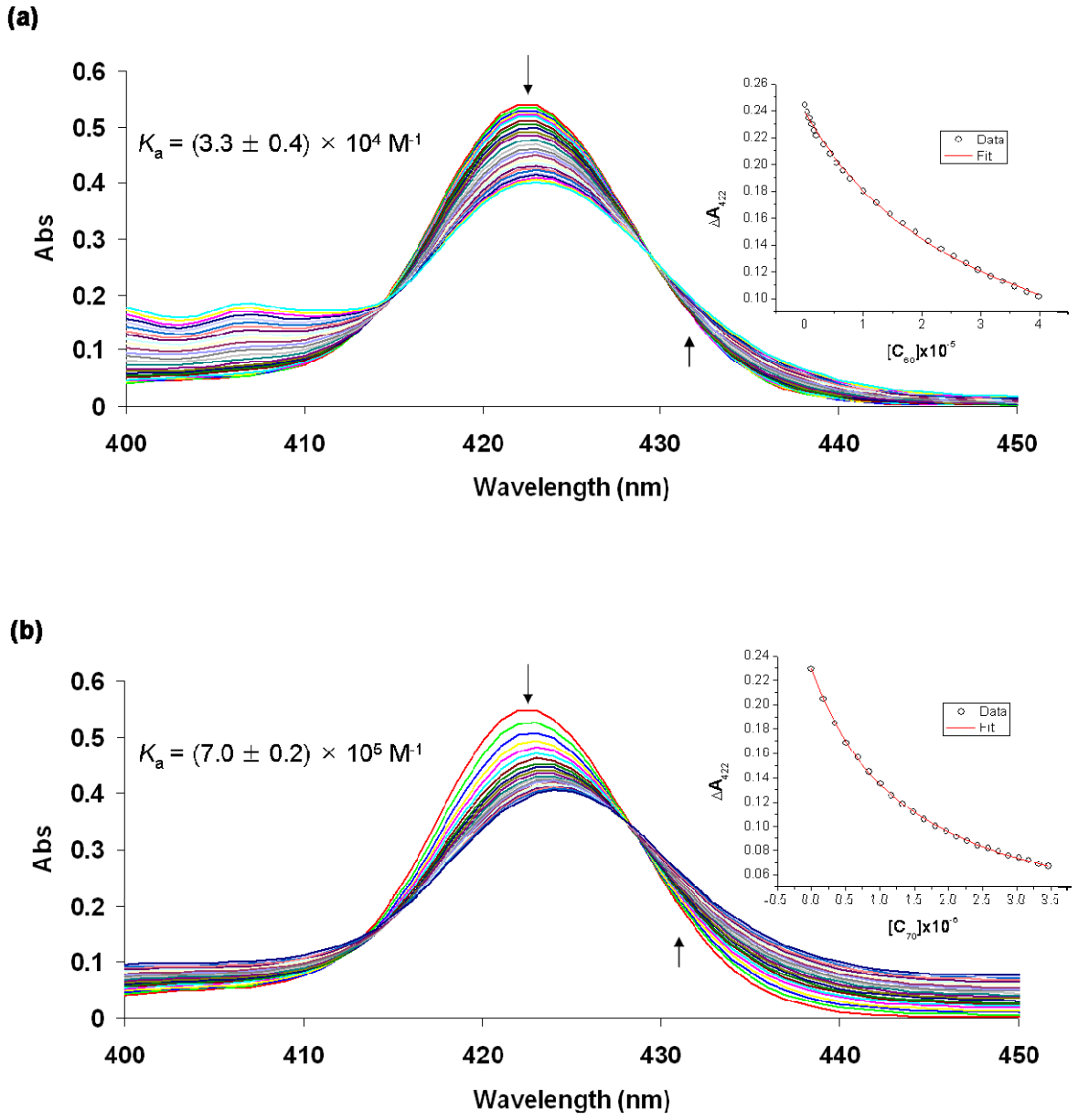

Fig. S6 Absorption spectra of **A1** (0.5×10^{-6} M) in toluene at 296 K upon titration with (a) C_{60} and (b) C_{70}. Insets: the absorption changes at 422 nm and the result of fitting the experimental data.

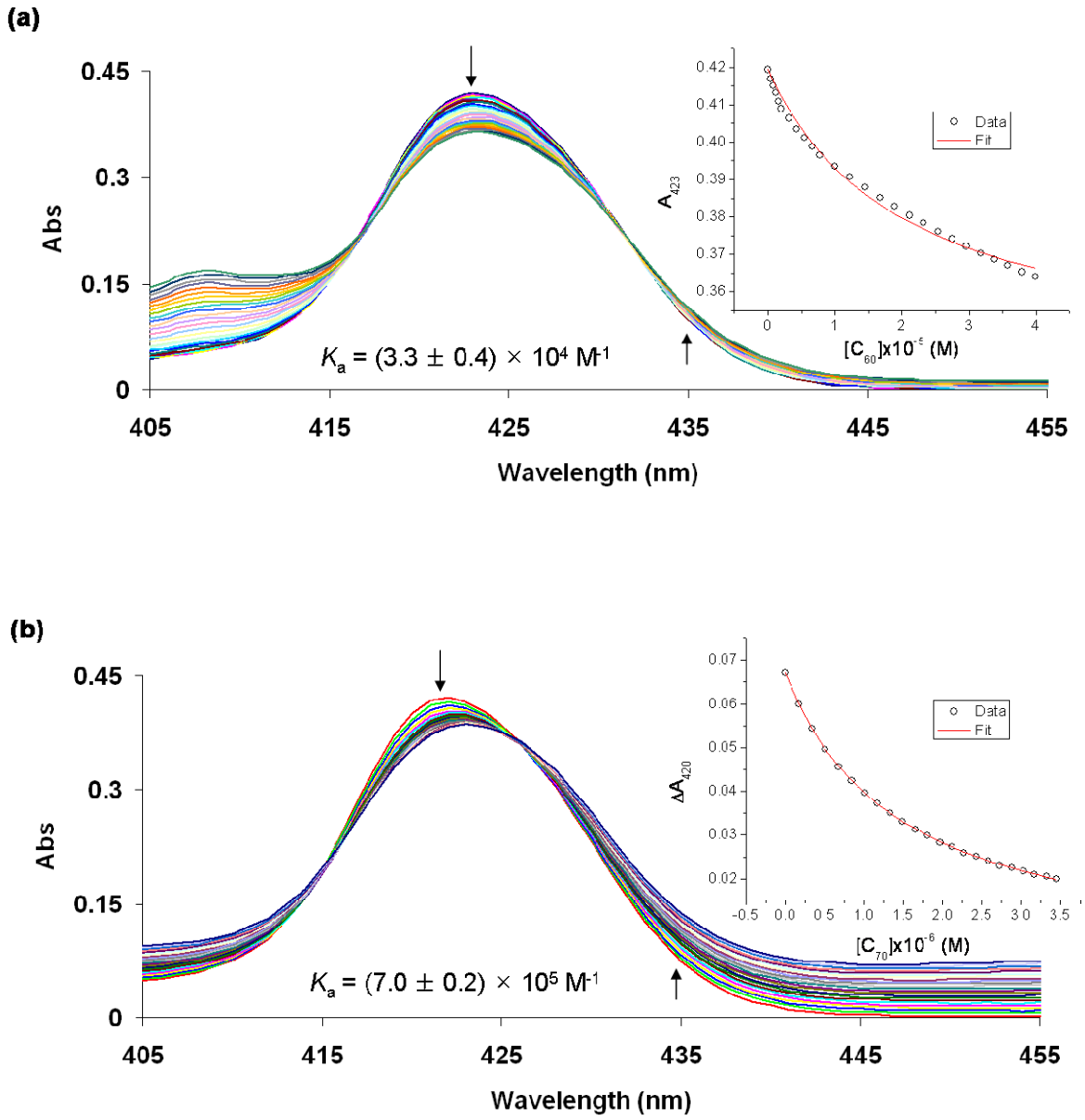

Fig. S7 Absorption spectra of **A2** (0.5×10^{-6} M) in toluene at 296 K upon titration with (a) C_{60} and (b) C_{70}. Insets: the absorption changes at (a) 423 and (b) 420 nm and the result of fitting the experimental data.

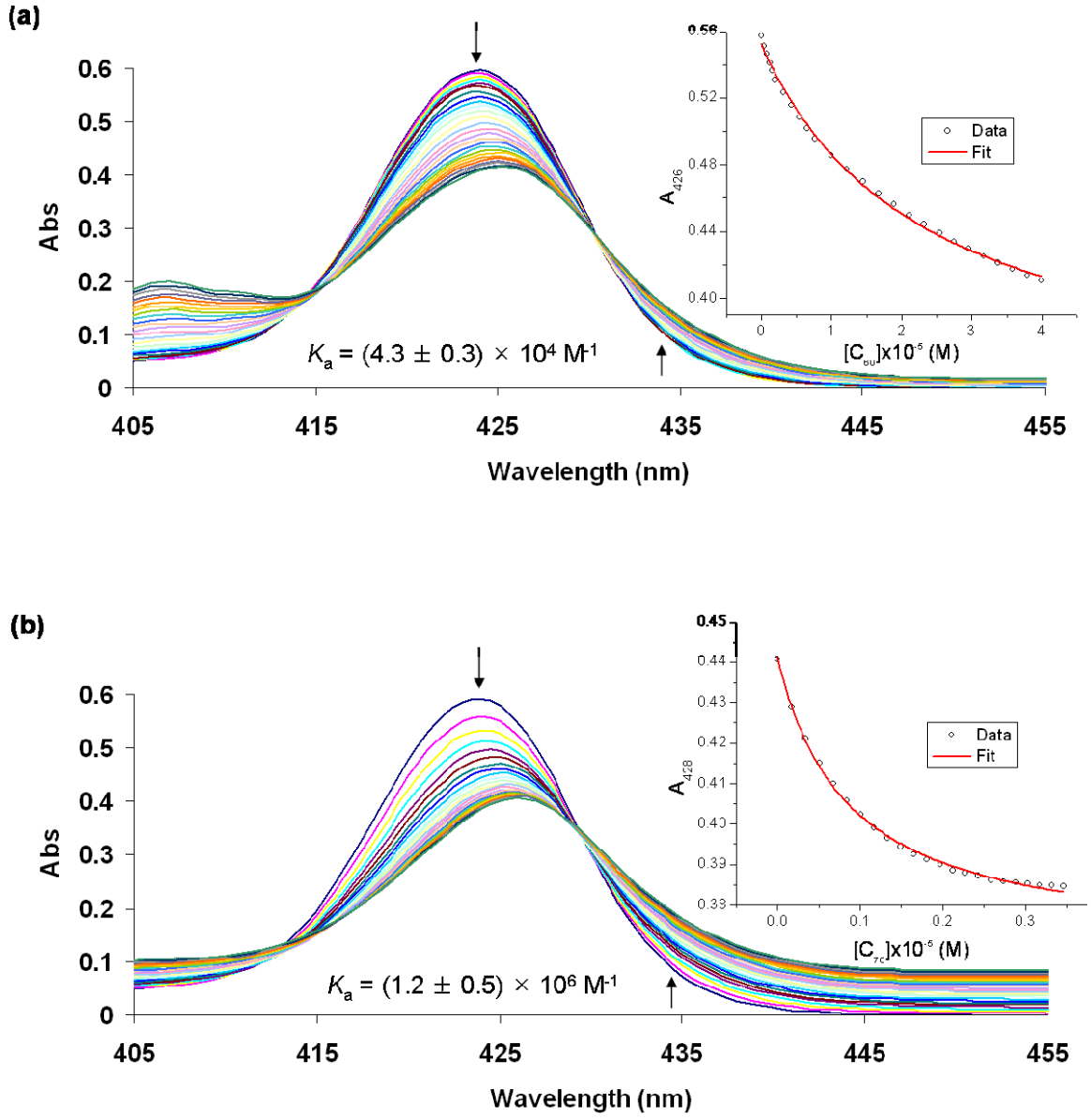

Fig. S8 Absorption spectra of **A3** (0.5×10^{-6} M) in toluene at 296 K upon titration with (a) C_{60} and (b) C_{70}. Insets: the absorption changes at (a) 426 and (b) 428 nm and the result of fitting the experimental data.

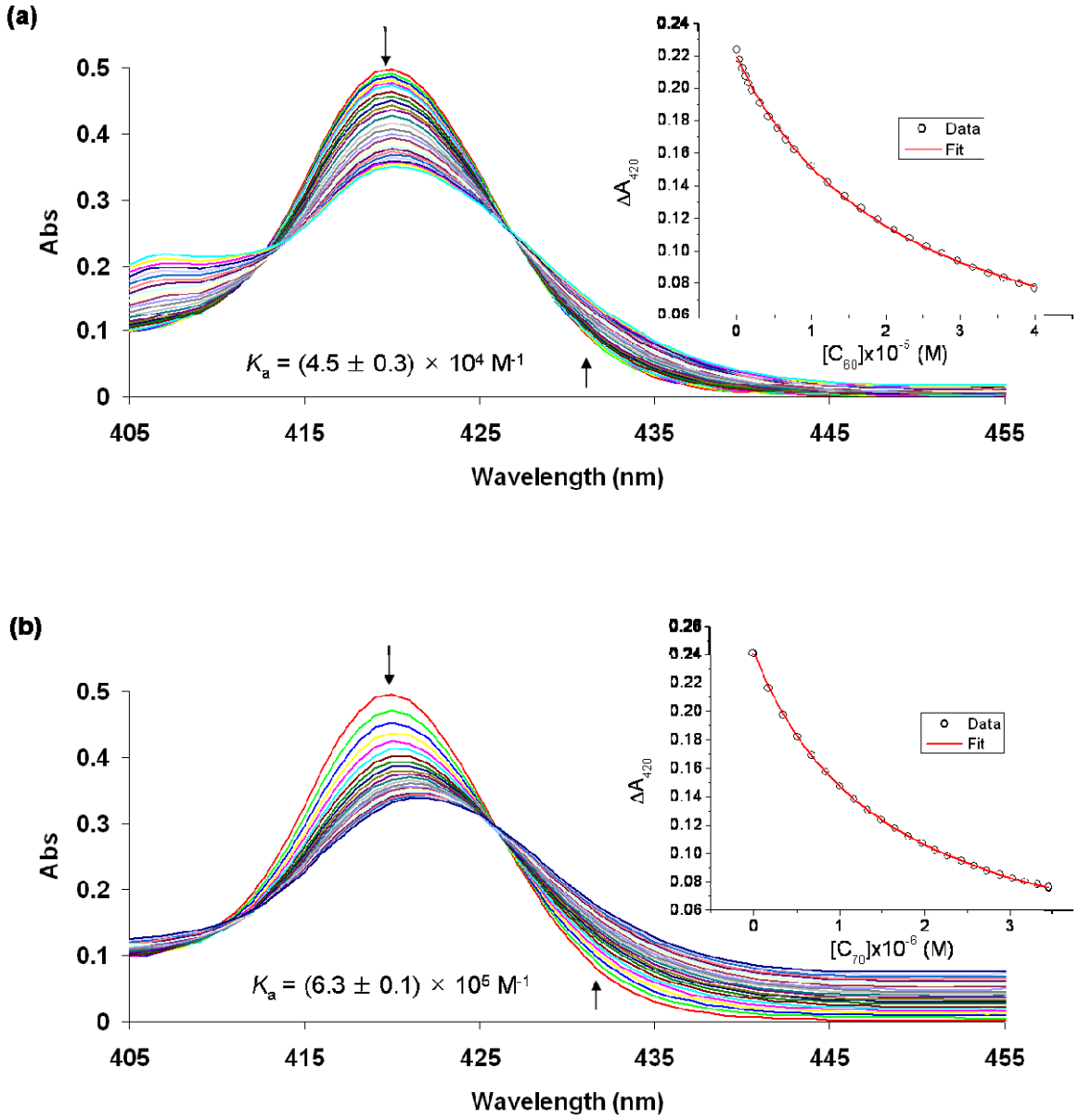

Fig. S9 Absorption spectra of **A4** (0.5×10^{-6} M) in toluene at 296 K upon titration with (a) C_{60} and (b) C_{70}. Insets: the absorption changes at 420 nm and the result of fitting the experimental data.

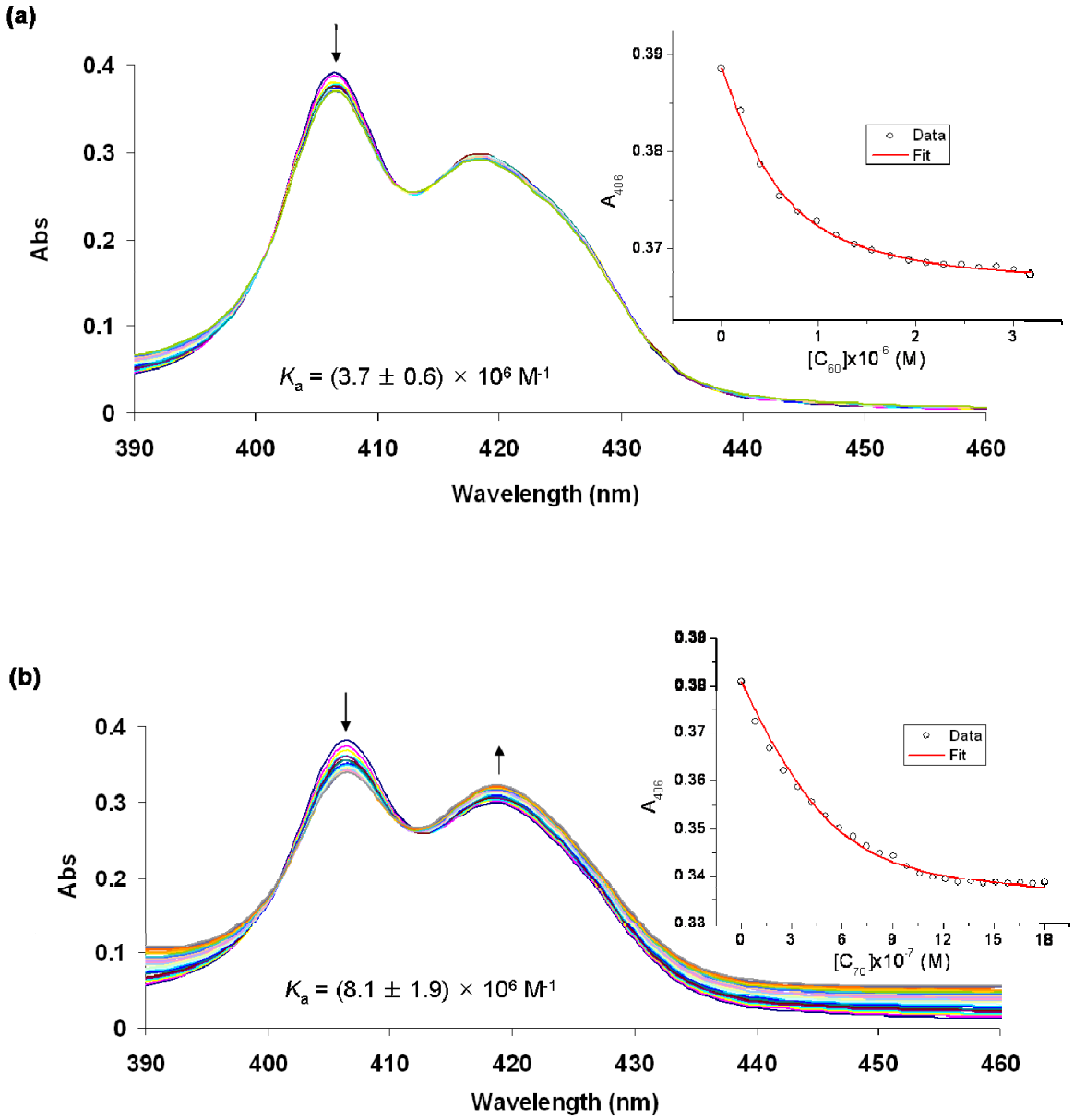

Fig. S10 Absorption spectra of **A5** (0.5 × 10^{-6} M) in toluene at 296 K upon titration with (a) C_{60} and (b) C_{70}. Insets: the absorption changes at 406 nm and the result of fitting the experimental data.

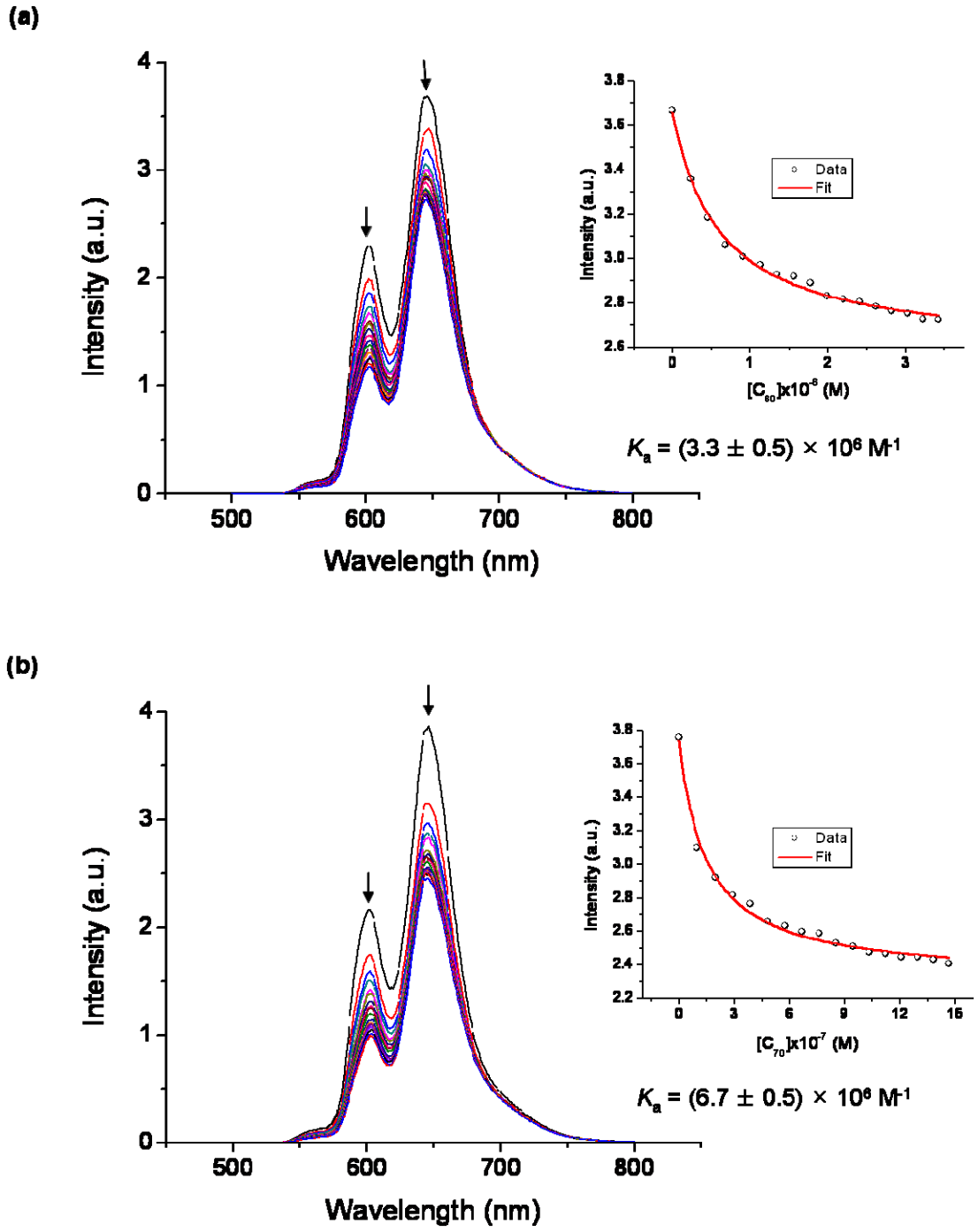

Fig. S11 Fluorescence spectra of **A5** (0.5×10^{-6} M) in toluene at 296 K upon titration with (a) C_{60} and (b) C_{70}. Insets: the fluorescence emission changes at (a) 645 and (b) 649 nm and the result of fitting the experimental data.

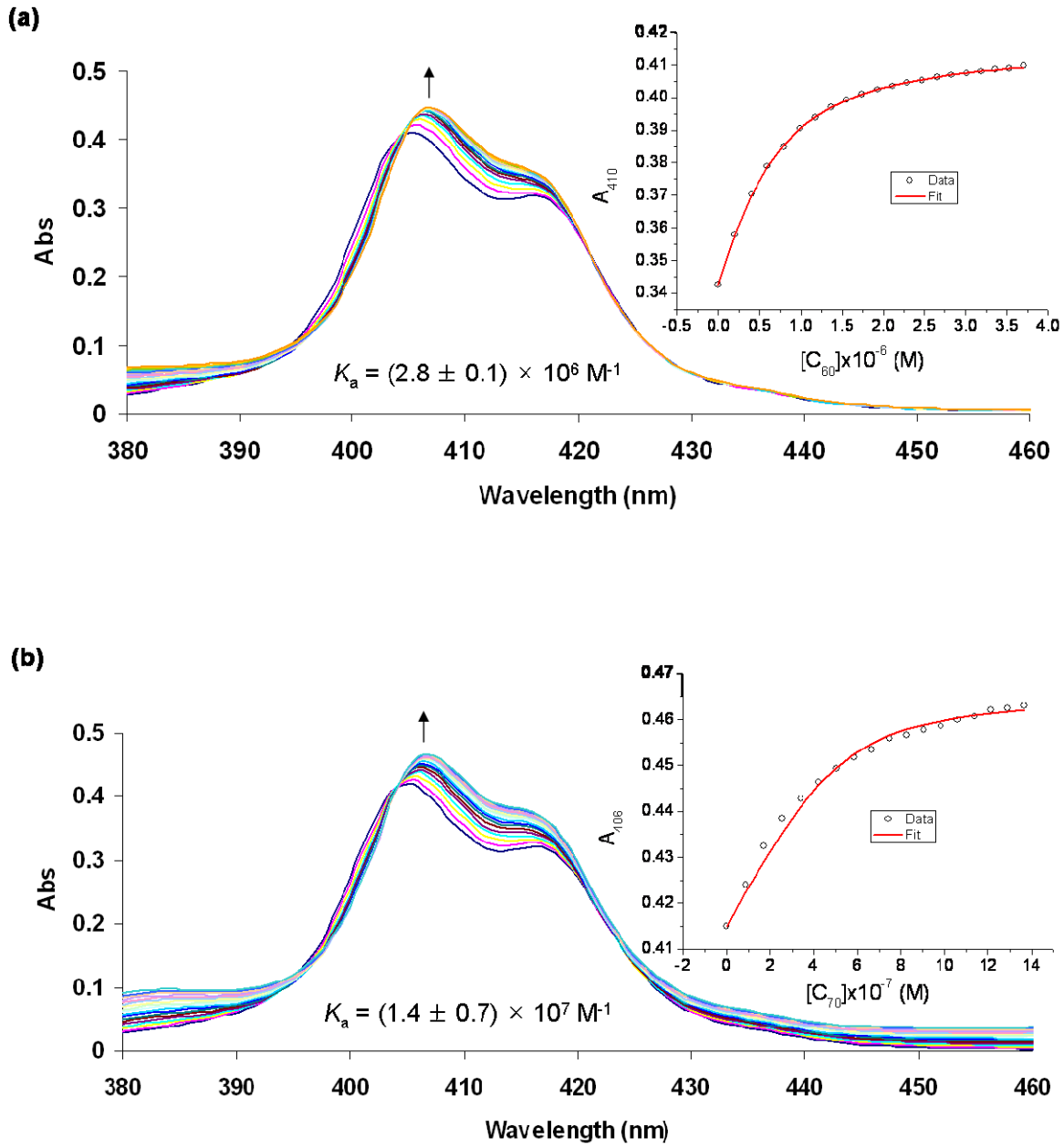

Fig. S12 Absorption spectra of **A6** (0.5 × 10^{-6} M) in toluene at 296 K upon titration with (a) C_{60} and (b) C_{70}. Insets: the absorption changes at (a) 410 and (b) 406 nm and the result of fitting the experimental data.

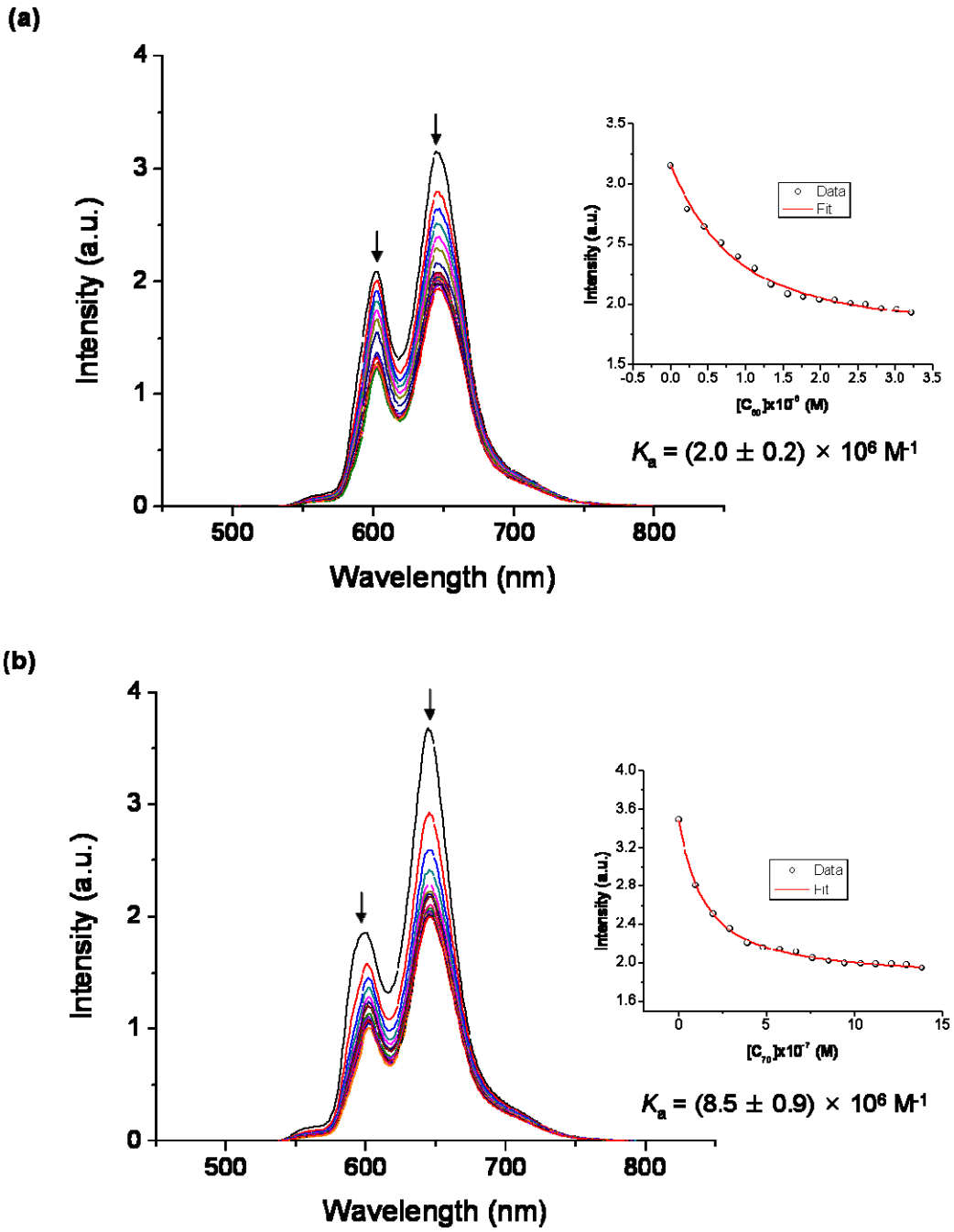

Fig. S13 Fluorescence spectra of **A6** (0.5×10^{-6} M) in toluene at 296 K upon titration with (a) C_{60} and (b) C_{70}. Insets: the fluorescence emission changes at (a) 645 and (b) 649 nm and the result of fitting the experimental data.

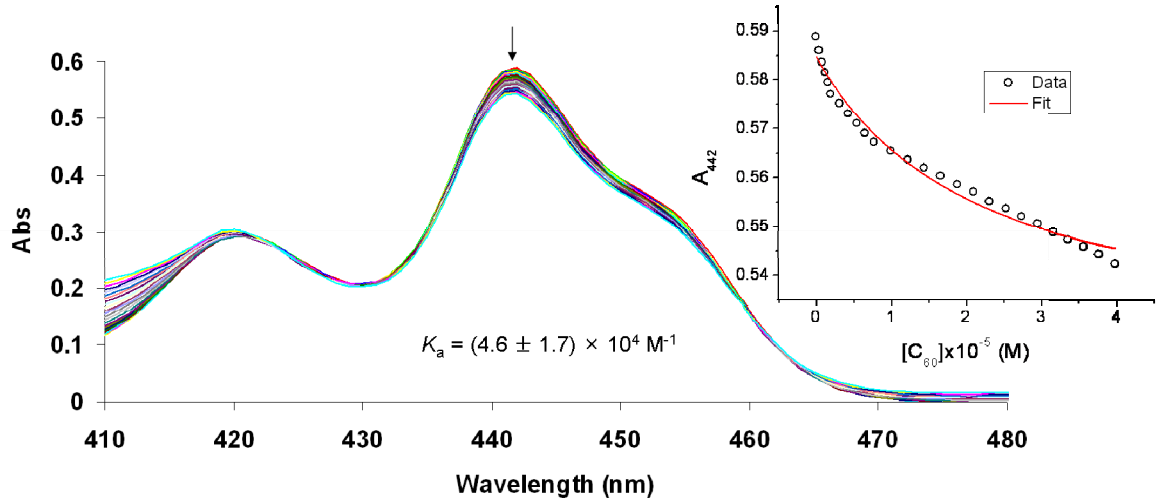

Fig. S14 Absorption spectra of **B1** (0.5×10^{-6} M) in toluene at 296 K upon titration with C_{60}. Inset: the absorption changes at 442 nm and the result of fitting the experimental data.

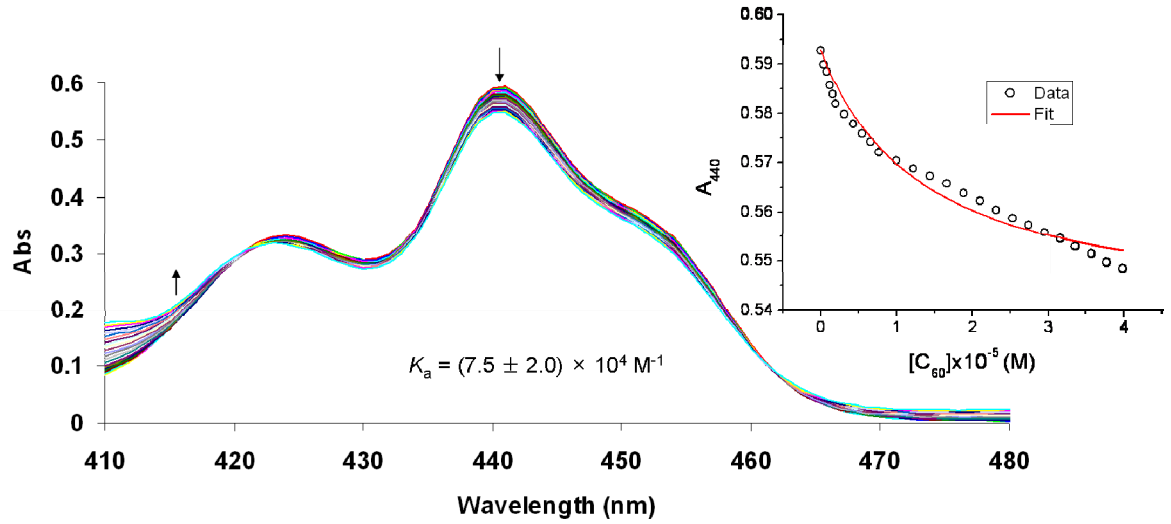

Fig. S15 Absorption spectra of **B2** (0.5×10^{-6} M) in toluene at 296 K upon titration with C_{60}. Inset: the absorption changes at 440 nm and the result of fitting the experimental data.

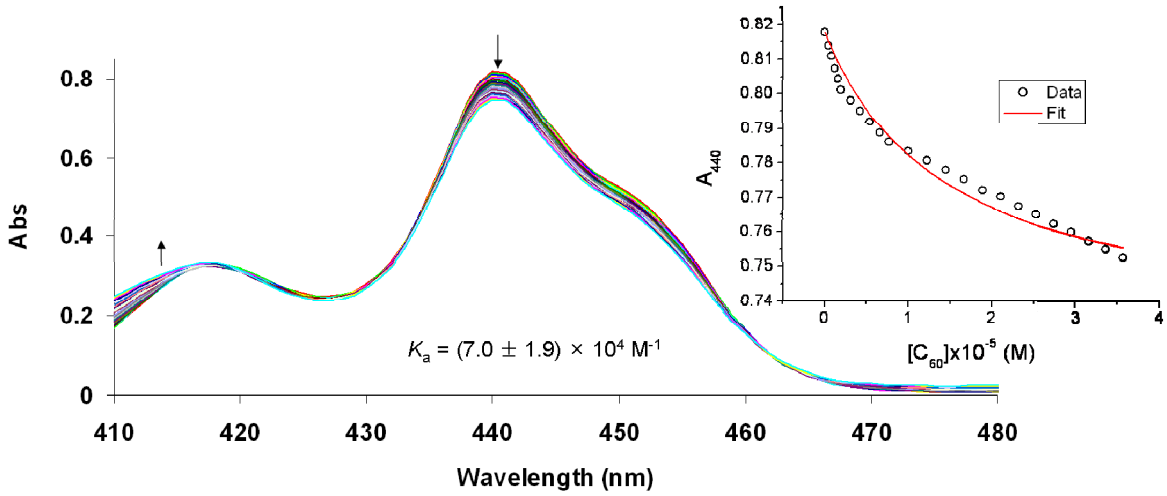

Fig. S16 Absorption spectra of **B3** (0.5×10^{-6} M) in toluene at 296 K upon titration with C_{60}. Inset: the absorption changes at 440 nm and the result of fitting the experimental data.

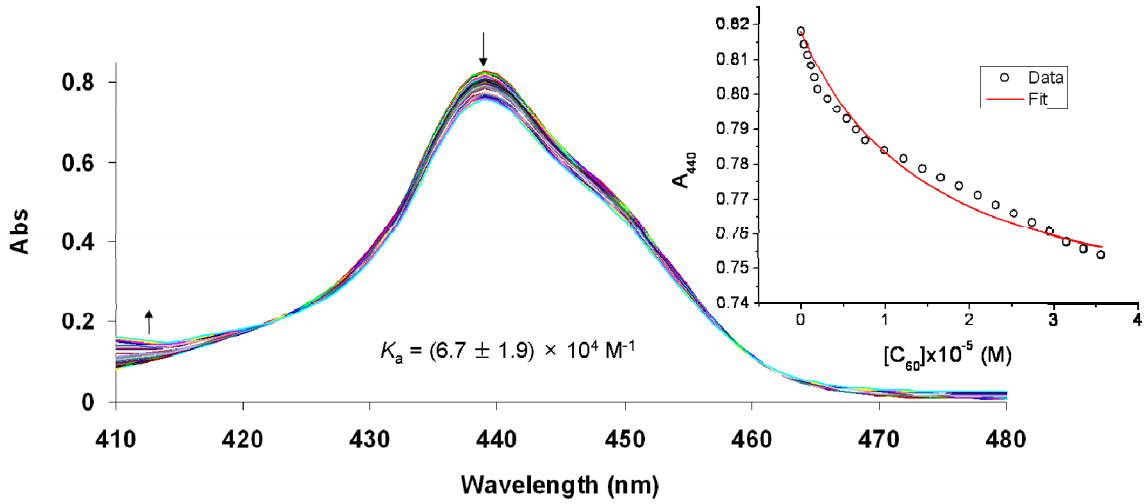

Fig. S17 Absorption spectra of **B4** (0.5×10^{-6} M) in toluene at 296 K upon titration with C_{60}. Inset: the absorption changes at 440 nm and the result of fitting the experimental data.

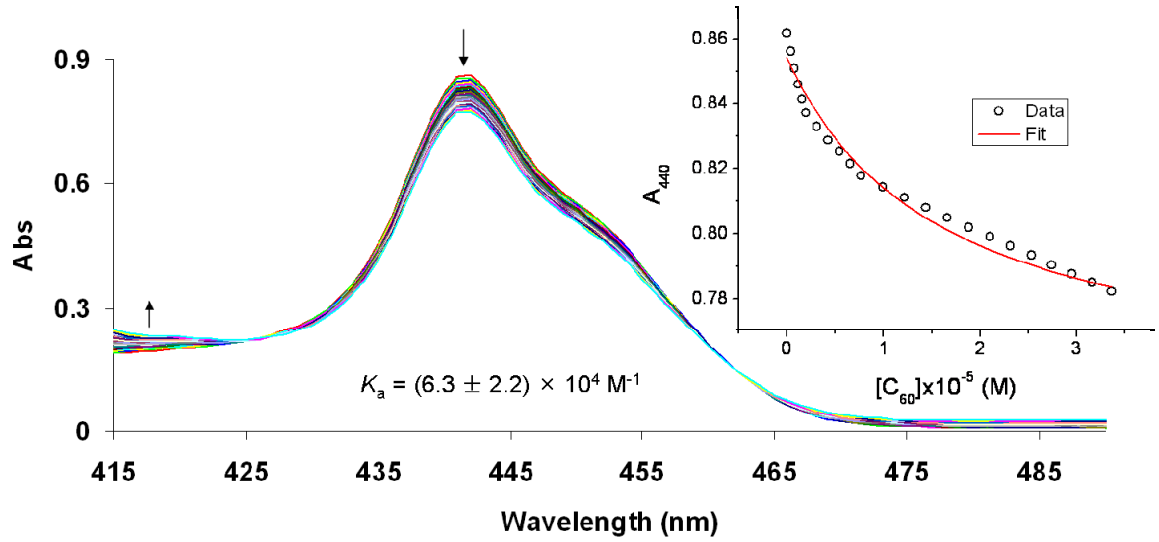

Fig. S18 Absorption spectra of **B5** (0.5×10^{-6} M) in toluene at 296 K upon titration with C_{60}. Inset: the absorption changes at 440 nm and the result of fitting the experimental data.

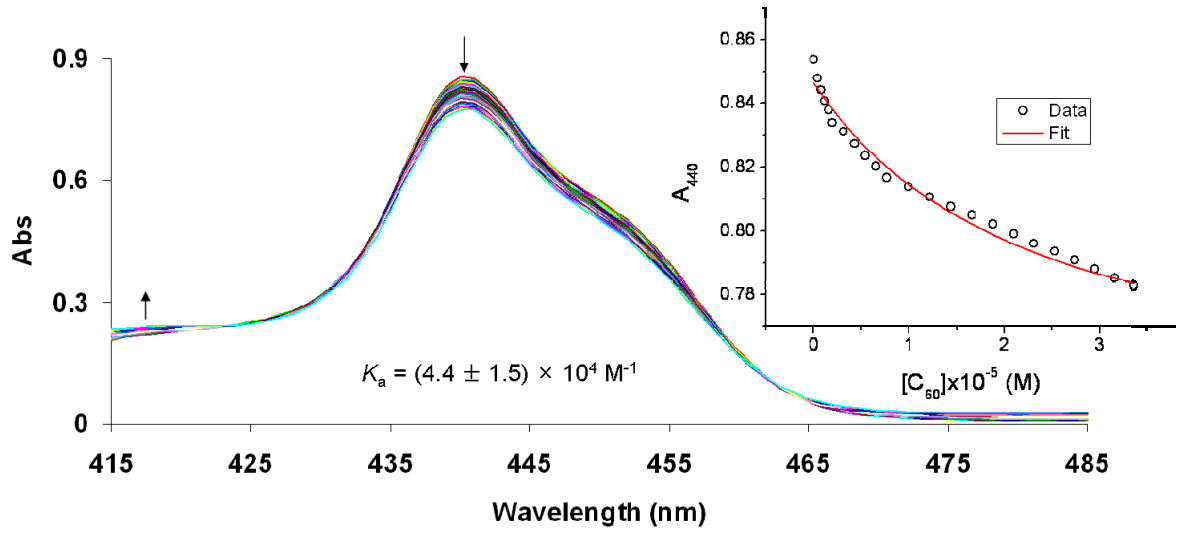

Fig. S19 Absorption spectra of **B6** (0.5×10^{-6} M) in toluene at 296 K upon titration with C_{60}. Inset: the absorption changes at 440 nm and the result of fitting the experimental data.

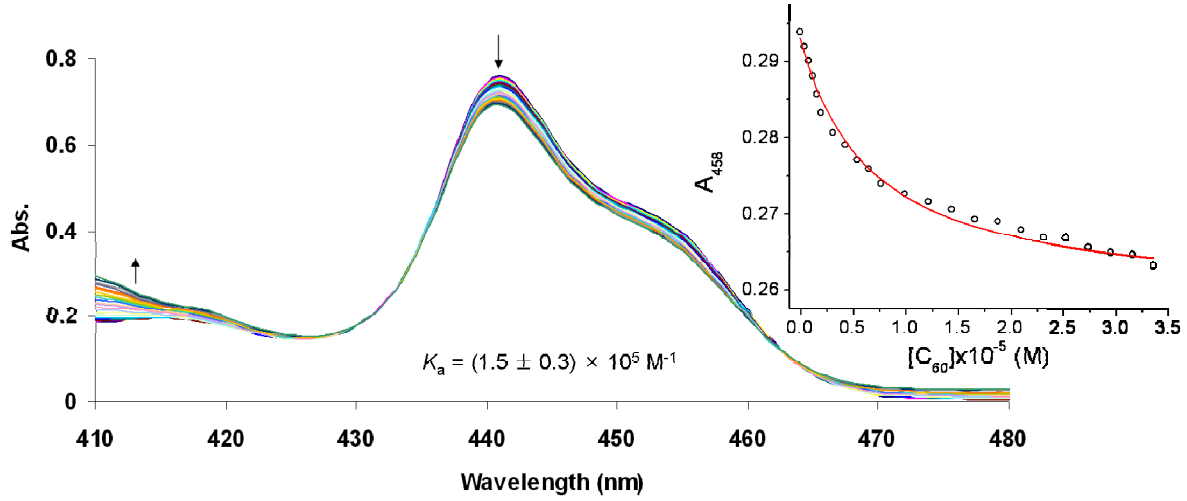

Fig. S20 Absorption spectra of **B7** (0.5×10^{-6} M) in toluene at 296 K upon titration with C_{60}. Inset: the absorption changes at 458 nm and the result of fitting the experimental data.

VI. Variable-temperature ^{13}C NMR experiments.

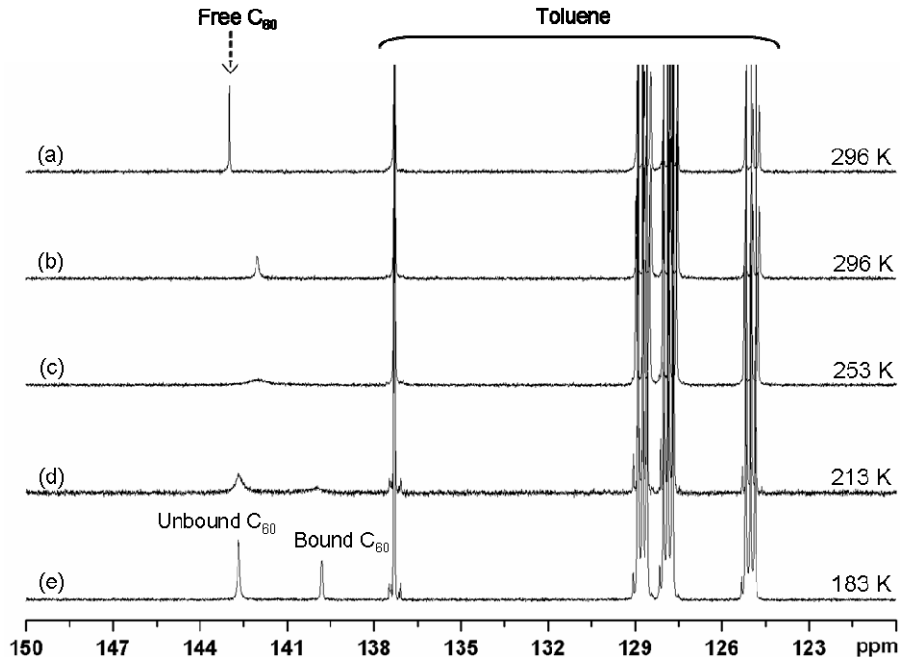

Fig. S21 Variable-temperature ^{13}C NMR spectra of ^{13}C-enriched C_{60} in the (a) absence or (b-e) presence of **A1** (0.33 equiv) in toluene-d_8.

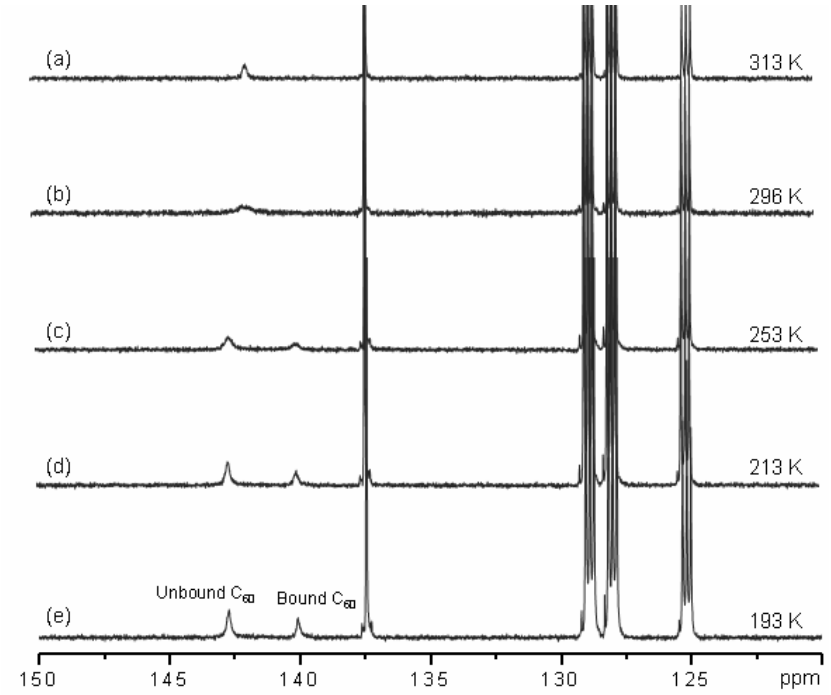

Fig. S22 Variable-temperature ^{13}C NMR spectra of ^{13}C-enriched C_{60} in the presence of **A6** (0.33 equiv) in toluene-d_8.

VII. The geometry optimizations for Zn(porphyrin) dimer A2 and bisected Zn(porphyrin) tetramer B2. Ab intio quantum mechanical calculations were carried out using Spartan'08 for Windows on an Intel Core i5 CPU Studio 1569 laptop running Windows 7 operating system.[S16] To facilitate geometry optimization, the ^{n}hexyl group of bisected Zn(porphyrin) tetramer **B2** was replaced by H atom. The geometry optimizations (equilibrium geometries) for each complex at the ground state were performed with the 3-21G basis set, using the Hartree-Fock method (HF).

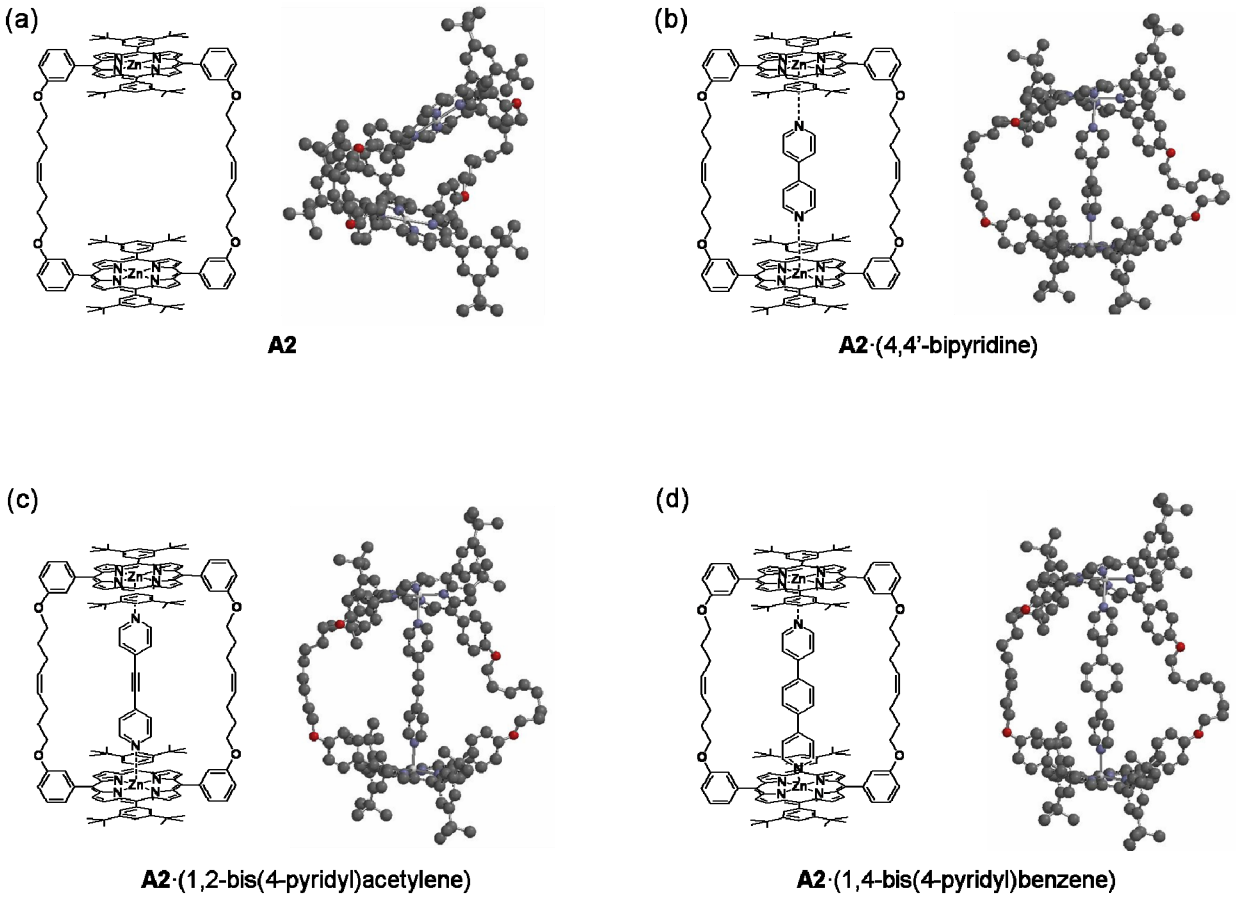

Fig. S23 Optimized HF geometries for: (a) dimer **A2**, (b) **A2**·(4,4'-bipyridine), (c) **A2**·(1,2-bis(4-pyridyl)acetylene), and (d) **A2**·(1,4-bis(4-pyridyl)benzene) structures.

Table S1. Zn-Zn distances and total energies for dimer **A2**, **A2**·(4,4'-bipyridine), **A2**·(1,2-bis(4-pyridyl)acetylene), and **A2**·(1,4-bis(4-pyridyl)benzene) structures.

	A2	**A2**·(4,4'-bipyridine)	**A2**·(1,2-bis(4-pyridyl)acetylene)	**A2**·(1,4-bis(4-pyridyl)benzene)
Zn-Zn distance (Å) × minimum horizontal distance (Å)	8.4 × 24.3	11.4 × 18.3	13.8 × 16.7	15.6 × 14.7
Total energy (kJ/mol)	-950	-1925	-1893	-2061

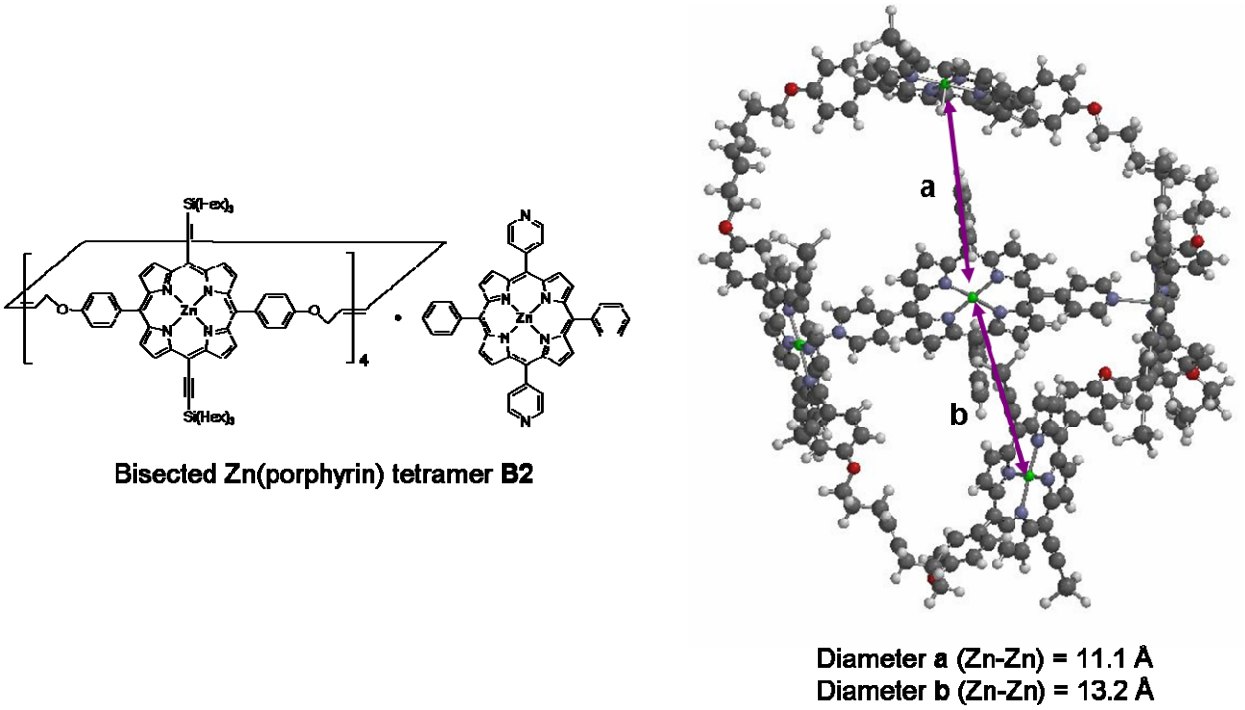

Fig. S24 Optimized HF geometry of the bisected Zn(porphyrin) tetramer **B2** structure.

VIII. Author contributions audit: B.K. and S.T.N. conceived the experiments presented herein based on a suggestion from J.T.H.. B.K. and R.K.T. synthesized and characterized all compounds. B.K. carried out the UV-vis and fluorescence titration experiments. R.K.T. carried out the variable-temperature ^{13}C NMR experiments. M.H.W. performed the geometrical optimization of porphyrin assemblies using Spartan'08. S.T.N. supervised the project. B.K. wrote the initial draft of the paper and received inputs and corrections from all co-authors. B.K., R.K.T., and S.T.N. finalized the manuscript.

IX. References

S1 R. K. Totten, P. Ryan, B. Kang, S. J. Lee, L. J. Broadbelt, R. Q. Snurr, J. T. Hupp and S. T. Nguyen, *Chem. Commun.* 2012, **48**, 4178-4180.

S2 B. Kang, J. W. Kurutz, K.-T. Youm, R. K. Totten, J. T. Hupp and S. T. Nguyen, *Chem. Sci.* 2012, **3**, 1938-1944.

S3 E. B. Fleischer and A. M. Shachter, *Inorg. Chem.* 1991, **30**, 3763-3769.

S4 J. Fan, J. A. Whiteford, B. Olenyuk, M. D. Levin, P. J. Stang and E. B. Fleischer, *J. Am. Chem. Soc.* 1999, **121**, 2741-2752.

S5 B. Steiger, C. Shi and F. C. Anson, *Inorg. Chem.* 1993, **32**, 2107-2113.

S6 A. B. Pangborn, M. A. Giardello, R. H. Grubbs, R. K. Rosen and F. J. Timmers, *Organometallics* 1996, **15**, 1518-1520.

S7 C. He, Q. He, C. Deng, L. Shi, D. Zhu, Y. Fu, H. Cao and J. Cheng, *Chem. Commun.* 2010, **46**, 7536-7538.

S8 Y. Shoji, K. Tashiro and T. Aida, *J. Am. Chem. Soc.* 2006, **128**, 10690-10691.

S9 OriginPro 8.0, OriginLab Corp., Northampton, MA, USA.

S10 P. D. W. Boyd and C. A. Reed, *Acc. Chem. Res.* 2005, **38**, 235-242.

S11 K. Tashiro and T. Aida, *Chem. Soc. Rev.* 2007, **36**, 189-197.

S12 A. Hosseini, S. Taylor, G. Accorsi, N. Armaroli, C. A. Reed and P. D. W. Boyd, *J. Am. Chem. Soc.* 2006, **128**, 15903-15913.

S13 G. Gil-Ramírez, S. D. Karlen, A. Shundo, K. Porfyrakis, Y. Ito, G. A. D. Briggs, J. J. L. Morton and H. L. Anderson, *Org. Lett.* 2010, **12**, 3544-3547.

S14 L. P. Hernández-Eguía, E. C. Escudero-Adán, I. C. Pintre, B. Ventura, L. Flamigni and P. Ballester, *Chem.—Eur. J.* 2011, **17**, 14564-14577.

S15 L. P. Hernández-Eguía, E. C. Escudero-Adán, J. R. Pinzón, L. Echegoyen and P. Ballester, *J. Org. Chem.* 2011, **76**, 3258-3265.

S16 *Spartan'08 for Windows*; Wavefunction, Inc. Irvine, CA, 2008.